Effect of Vorticity on Peregrine Breather for Interfacial Waves of Finite Amplitude

Shibam Manna and Asoke Kumar Dhar

1 Introduction

The stability of two-dimensional (2D) finite amplitude steady waves to arbitrary small 3D perturbations on the surface of infinite depth of water has been analysed numerically by Maclean et al. [1]. This analysis discloses that there are two different types of instabilities for finite amplitude gravity waves. The first is predominantly 2D and is associated with all the known results for particular cases as for example Benjamin–Feir instability. The second is predominantly 3D and becomes dominant when the steepness of the wave is very large. This work in the case of interfacial waves is then extended by Yuen [2]. The 2D instability of interfacial gravity waves in the particular case of long wave length perturbation and small wave steepness has been studied analytically by Grimshaw and Pullin [3] from the cubic NLSE. Later, Pullin and Grimshaw [4] have extended this analysis for interfacial gravity waves including the effect of basic current shear in the superposition of either or both the inviscid fluids and have reported both the analytical and numerical results. Later on, Dhar and Das [5] analysed the stability of gravity interfacial waves of infinite depth including the effect of shear current. There are many cases in which we observed that currents are not uniform with the water depth. In view of the above, many situations such as air–water interfaces and jet-like ebb flows can be cited, which incorporates non-uniformity of the currents with depth. In the presence of linear shear current for which velocity is uniform, it was theoretically observed that the motion of the wave continues to be irrotational and also constant vorticity can only effect the dispersion relation at first order of approximation. Choi [6] applied a pseudospectral process to analyse the interaction of nonlinear surface

S. Manna (✉) · A. K. Dhar
Indian Institute of Engineering Science and Technology, Shibpur, India
e-mail: fake5@nodycon2021.it

W. Lacarbonara et al. (eds.), *Advances in Nonlinear Dynamics*, NODYCON Conference Proceedings Series, https://doi.org/10.1007/978-3-030-81170-9_41

gravity waves including linear shear currents and observed that the maximum wave amplitude for positive shear current is much smaller than that in the absence of any shear, while the effect reverse to this is found for a negative shear current. A fully nonlinear boundary integral method to present the interaction between gravity waves and shear currents including the arbitrary distribution of vorticity was suggested by Nwogu [7]. He observed that the vorticity can significantly affect the development of modulated wave trains. It is to be noted that for analysing the nonlinear evolution of water waves, nonlinear Schrodinger equations are generally applied due to its proper reflection of modulational instability. Ever since the experimental validation of the analytical soliton like solution of NLSE, there has been much of an interest shown by the researchers towards the Peregrine Breather [8] like solution of the NLSE. Considering the case of infinite depth superposed fluids, the instances of air–water interface as well as the Boussinesq approximation have been analysed in that paper. According to Liao et al. [9], being a theoretical solution of third-order NLSE, the PB can be viewed as a prototype of Rogue waves and as such the impact of basic current shear for finite amplitude interfacial waves on PB is of considerable interest of this paper. In this chapter, we first derived a third-order NLSE for a gravity wave travelling at the interface of two superposed fluids having finite depths including the effect of basic current shear. From this evolution equation, we then performed a stability analysis in the cases of air–water interface as well as the Boussinesq approximation. Later, the effect of vorticity on Peregrine Breather has also been examined.

2 Governing Equations

We consider the interface between two inviscid and incompressible fluids in the perturbed state by the equation $y = \zeta(x, t)$. The two fluids having densities ρ_1 and ρ_2 ($\rho_1 < \rho_2$), respectively, are bounded by the horizontal planes at $y = h_1$ and $y = -h_2$. In each fluid, the basic current has constant vorticity ω_1 and ω_2, respectively. As three space dimensional perturbations to the primary wave are not vorticity preserving, the stability analysis presented here is limited to two space dimensional that can be considered as irrotational. Now, we employ the following transformations for dimensionless variables:

$$\sqrt{k_0^3/g}(\phi, \phi', \psi, \psi') \to (\phi, \phi', \psi, \psi'), \quad k_0(x, y, \zeta, h_1, h_2) \to (x, y, \zeta, h_1, h_2),$$
$$\sqrt{1/k_0 g}(\omega_1, \omega_2) \to (\omega_1, \omega_2), \quad \sqrt{k_0 g}t \to t, \quad r = \rho_1/\rho_2. \tag{1}$$

The governing equations can be expressed as

$$\nabla^2\phi' = 0, \quad \nabla^2\psi' = 0, \quad \text{in } \zeta < y < h_1 \tag{2}$$

$$\nabla^2\phi = 0, \quad \nabla^2\psi = 0, \quad \text{in } -h_2 < y < \zeta \tag{3}$$

$$\phi'_y - \zeta_t = (\phi'_x - \omega_1\zeta)\zeta_x, \quad \text{for } y = \zeta \tag{4}$$

$$\phi_y - \zeta_t = (\phi_x - \omega_2\zeta)\zeta_x, \quad \text{for } y = \zeta \tag{5}$$

$$\begin{aligned}\phi_t - r\phi'_t + (1-r)\zeta + \omega_2\psi - r\omega_1\psi' \\ = \frac{r}{2}(\nabla\phi')^2 - \frac{1}{2}(\nabla\phi)^2 + \omega_2 y\phi_x - r\omega_1 y\phi'_y, \quad \text{for } y = \zeta\end{aligned} \tag{6}$$

$$\phi_y = 0, \ \psi = 0, \ \text{on } y = -h_2 \text{ and } \phi'_y = 0, \ \psi' = 0, \ \text{on } y = h_1, \tag{7}$$

where ψ' and ψ are the stream functions for the upper and lower fluids satisfying the Cauchy–Riemann relations as follows:

$$\phi'_x = \psi'_y, \ \ \phi'_y = -\psi'_x, \ \ \phi_x = \psi_y, \ \ \phi_y = -\psi_x. \tag{8}$$

A solution can be found in the following form:

$$P = P_0 + \sum_{n=1}^{\infty}[P_n \exp\{in(kx - \sigma t)\} + c.c.], \tag{9}$$

where P symbolises for ϕ', ϕ, ψ', ψ, ζ, and "c.c." means complex conjugate. Here $\phi'_n, \phi_n, \psi'_n, \psi_n$ $(n = 0, 1, 2)$ are functions of $y, x_1 = \epsilon x, t_1 = \epsilon t$, whereas the ζ_n are functions of x_1, t_1, and ϵ is a slow ordering parameter. The linear dispersion relation for a plane progressive wave is given by

$$f(\sigma, k) = \sigma_1\sigma^2 + r\sigma_2\sigma^2 - (\omega_2 - r\omega_1)\sigma\sigma_1\sigma_2 - k(1-r)\sigma_1\sigma_2, \tag{10}$$

where $\sigma_i = \tanh kh_i, \quad (i = 1, 2)$. We assume that the primary wave has the wave number k_0. Therefore, we have $k = 1$, and the relation (10) for finding σ thus reduces to

$$(\sigma_1 + r\sigma_2)\sigma^2 - (\omega_2 - r\omega_1)\sigma\sigma_1\sigma_2 - (1-r)\sigma_1\sigma_2 = 0. \tag{11}$$

From the dispersion relation, the group velocity c_g of the primary wave can be found as

$$c_g = \frac{-\delta_0\sigma^2 + \{(\omega_2 - r\omega_1)\sigma + (1-r)\}\delta_1 + (1-r)\sigma_1\sigma_2}{2(\sigma_1 + r\sigma_2)\sigma - (\omega_2 - r\omega_1)\sigma_1\sigma_2}, \tag{12}$$

where $\delta_0 = h_1(1-\sigma_1^2) + rh_2(1-\sigma_2^2)$ and $\delta_1 = \sigma_1 h_2(1-\sigma_2^2) + \sigma_2 h_1(1-\sigma_1^2)$.

3 Derivation of Evolution Equation

By inserting the expansions of (9) into (2) and (3), we obtain the following solutions:

$$\phi'_n = \text{sech}\,(h_1 k_n)\cosh[(y-h_1)k_n]C'_n, \quad \psi'_n = \text{sech}\,(h_1 k_n)\sinh[(y-h_1)k_n]D'_n, \tag{13}$$

$$\phi_n = \text{sech}\,(h_2 k_n)\cosh[(y+h_2)k_n]C_n, \quad \psi_n = \text{sech}\,(h_2 k_n)\sinh[(y+h_2)k_n]D_n, \tag{14}$$

where C'_n, D'_n C_n, D_n, $(n = 1, 2)$ are functions of x_1, t_1 and $k_n = n - i\epsilon\frac{\partial}{\partial x_1}$. For $n = 0$, we get the solutions of zeroth harmonic terms after taking Fourier transforms of (2) and (3)

$$\overline{\phi'_0} = \text{sech}\,(h_1\epsilon\bar{k})\cosh[(y-h_1)\epsilon\bar{k}]C'_0, \quad \overline{\psi'_0} = \text{sech}\,(h_1\epsilon\bar{k})\sinh[(y-h_1)\epsilon\bar{k}]D'_0, \tag{15}$$

$$\overline{\phi_0} = \text{sech}\,(h_2\epsilon\bar{k})\cosh[(y+h_2)\epsilon\bar{k}]C_0, \quad \overline{\psi_0} = \text{sech}\,(h_2\epsilon\bar{k})\sinh[(y+h_2)\epsilon\bar{k}]D_0, \tag{16}$$

in which $\overline{\phi'_0}$, $\overline{\phi_0}$, $\overline{\psi'_0}$, $\overline{\psi_0}$ represent the Fourier transforms of the corresponding quantities defined by

$$(\overline{\phi'_0}, \overline{\phi_0}, \overline{\psi'_0}, \overline{\psi_0}) = \iint_{-\infty}^{\infty} (\phi'_0, \phi_0, \psi'_0, \psi_0)\mathrm{e}^{-i(\bar{k}x_1 - \bar{\sigma}t_1)}\,\mathrm{d}x_1\mathrm{d}t_1, \tag{17}$$

in which C'_0, D'_0, C_0, D_0 are functions of $\bar{k}$, $\bar{\sigma}$.

To solve three sets of equations corresponding to $n = 1, 2, 0$, we consider the perturbation expansion as follows:

$$F_m = \sum_{n=1}^{\infty} \epsilon^n F_{mn}, \quad (m = 0, 1), \quad F_2 = \sum_{n=2}^{\infty} \epsilon^n F_{2n}, \tag{18}$$

where F_m represents C'_m, D'_m, C_m, D_m, ζ_m $(m = 0, 1, 2)$.

Inserting (18) in the three sets of equations and equating different powers of ϵ, we obtain a sequence of equations; from the first set $(n = 1)$ of equations, corresponding to (4) and (5), we obtain solutions of C'_{11}, C'_{12}, C_{11}, C_{12}, respectively. Similarly, from second set $(n = 2)$ and third set $(n = 0)$, corresponding to (4), (5) and (2), we obtain solutions of C'_{22}, C_{22}, ζ_{22} and C'_{01}, C'_{02}, C_{01}, C_{02}, ζ_{01}, ζ_{02}, respectively. It is to be noted that the coefficients of D'_n and D_n $(n = 1, 2, 0)$ can be expressed in terms of C'_n, C_n by using the Cauchy–Riemann relations (8). Finally,

the equation resulting from (2) of the first set of equations can be expressed in the form as follows:

$$f(W_1, K_1)\zeta_1 = -ir\sigma_2(W_1 + \omega_1\sigma_1)a_1 - i(W_1 - \omega_2\sigma_2)\sigma_1 b_1 - \sigma_1\sigma_2 K_1 c_1, \quad (19)$$

where $W_1 = \sigma + i\epsilon\frac{\partial}{\partial t_1}$, $K_1 = 1 - i\epsilon\frac{\partial}{\partial x_1}$ and a_1, b_1, c_1 are quantities due to nonlinear terms. Now, inserting solutions of several perturbed quantities that appear right side of (19), applying the transformations,

$$\xi = x_1 - c_g t_1, \quad \tau = \epsilon t_1 \quad (20)$$

and setting $\zeta = \zeta_1 = \zeta_{11} + \epsilon\zeta_{12}$, we obtain the following third-order nonlinear evolution equation:

$$i\zeta_\tau + \alpha\zeta_{\xi\xi} + \mu\zeta^2\zeta^* = 0, \quad (21)$$

in which the coefficients are available in the Appendix. It is to be noted that the nonlinear term μ of (21) comes from the interaction of primary wave with the wave-induced mean flow and the second harmonic, respectively.

4 Modulational Instability analysis

The solution of Eq. (21) is

$$\zeta = (\zeta_0/2)\exp(-i\Delta\sigma\tau), \quad (22)$$

where ζ_0 is a real number, and the frequency shift $\Delta\sigma$ due to nonlinearity is

$$\Delta\sigma = (\mu/4)\zeta_0^2. \quad (23)$$

We now introduce the perturbation on the above solution given by

$$\zeta = (\zeta_0/2)(1 + \zeta' + i\theta')\exp(-i\Delta\sigma\tau), \quad (24)$$

in which ζ' and θ' are small real perturbations of amplitude and phase, respectively. Next, we assume that $(\zeta', \theta') \propto \exp(-i\Omega\tau)$. Inserting (24) in (21), linearising with respect to ζ', θ' and taking the Fourier transformation of the resulting equations given by

$$(\overline{\zeta'}, \overline{\theta'}) = \int_{-\infty}^{\infty} (\zeta', \theta')\mathrm{e}^{(-i\lambda\xi)}\,\mathrm{d}\xi,$$

we obtain the nonlinear dispersion as follows:

$$\overline{R_1} = \sqrt{\overline{R_2}(\overline{R_2} - \zeta_0^2 \mu/2)}, \tag{25}$$

in which

$$\overline{R_1} = \Omega - c_g \lambda, \quad \overline{R_2} = \alpha \lambda^2. \tag{26}$$

There is an instability when

$$\lambda^2 < (\mu/2\alpha)\zeta_0^2. \tag{27}$$

At marginal stability, the perturbed wave number λ is given as

$$\lambda = \sqrt{\mu/2\alpha}\zeta_0. \tag{28}$$

If this condition (27) is satisfied, then the maximum growth rate is

$$G_r = \mu \zeta_0^2/4. \tag{29}$$

5 Effect of Vorticity on Peregrine Breather

The non-dimensional form of Eq. (21) is

$$i\frac{\partial \zeta'}{\partial \tau'} + \frac{\partial^2 \zeta'}{\partial \xi'^2} + 2|\zeta'|^2 \zeta' = 0, \tag{30}$$

which is obtained by employing the following transformations on the variables:

$$\xi' = \frac{1}{2}\tilde{\zeta}\sqrt{\frac{2\mu}{\alpha}}\xi, \quad \tau' = \frac{1}{2}\mu\tilde{\zeta}^2\tau, \quad \zeta' = \frac{\zeta}{\tilde{\zeta}}, \tag{31}$$

where ξ' denotes the normalised coordinate and the normalised time is denoted as τ'. The Peregrine Breather solution of Eq. (30) is

$$\zeta'(\xi', \tau') = \left[\frac{4(1 + 4i\tau')}{1 + 4\xi'^2 + 16\tau'^2} - 1\right] \exp(2i\tau'). \tag{32}$$

This solution (32) is localised in both space and time. Applying the transformation (31) in (32), we obtain the Peregrine solution in its dimensional form as

$$\zeta(x_1, t_1) = \widetilde{\zeta} \exp(i\mu\widetilde{\zeta}^2 t_1) \left[\frac{4\alpha(1 + 2i\mu\widetilde{\zeta}^2 t_1)}{\alpha + 2\mu\widetilde{\zeta}^2(x_1 - c_g t_1)^2 + 4\alpha\mu^2\widetilde{\zeta}^4 t_1^2} - 1 \right] \tag{33}$$

6 Discussion and Conclusions

A third-order NLSE is established for gravity waves travelling at the interface of two superposed fluids of finite depth under the circumstance of a shear current. Using this equation, the instability analysis is then investigated for air–water interface ($r = 0.00129$) as well as the Boussinesq approximation ($r \to 1$). Furthermore, the effect of vorticity on the peregrine breather has been taken into account. For an air–water interface from Fig. 1, we observed that G_r increases as $|\omega_1|$ decreases for fixed depth h_2 of the lower fluid, that is, the basic current shear in the air decreases G_r for fixed values of h_2. Also, for fixed $|\omega_1|$, G_r increases as h_2 increases. Now, from Fig. 2, we found that G_r increases as ω_2 decreases, but the reverse effect is observed for $-$ve vorticity. Also, for fixed +ve vorticity, G_r decreases as h_2 increases, and the reverse effect is observed for fixed values of $-$ve vorticity. Here, we found that sufficiently big value of the +ve basic current shear (ω_2) in the water removes the modulational instability for surface gravity waves of fixed finite depth of water, but $-$ve basic current shear increases G_r. For the case of Boussinesq approximation, we see from Fig. 3 that G_r increases with the increment of ω_1 for fixed values of h_1. In Fig. 4, we have plotted curves for several values of h_1, h_2, ω_1, ω_2 for both air–water interface and the Boussinesq approximation. As h_1, $h_2 \to \infty$, the four curves of Fig. 4 are similar as those of Dhar and Das [5]. Here, we see that the basic current shear in the air (ω_1) decreases G_r for surface waves of infinite depths. Furthermore, for $r \to 1$, which corresponds to potential oceanic or atmospheric application, we found that G_r increases as ω_1 increases for deep water surface gravity waves. For $r = 0.00129$ as well as $r \to 1$, wave number λ at marginal stability has been depicted in Fig. 5 for several values of h_1, h_2, ω_1, ω_2. For the case of air–water interface, from Fig. 6, we see that the breather span increases as h_2 decreases, while the breather span increases as $|\omega_1|$ increases. From Fig. 7, it is observed that h_1 has similar influence on breather span as that of the case in Fig. 6 for h_2 and the breather span increases for increasing +ve values of ω_2, while the reverse effect is encountered for $-$ve values of ω_2. For the Boussinesq approximation, Fig. 8 depicts that the span of the breather decreases as h_1 increases whereas the breather span decreases as ω_1 increases. In Fig. 9, we have plotted breather solution for several finite values of h_1, h_2, ω_1, ω_2. From Figs. 10 and 11 for air–water interface, we find that for fixed value of ω_1, ω_2, the breather width increases both in space and in time as h_2 decreases. In Figs. 12 and 13, we have plotted the breather solution for several

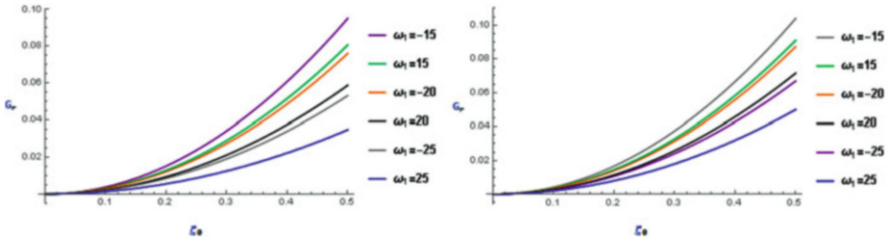

Fig. 1 G_r vs. ζ_0 plot for $r = 0.00129$, $h_1 \to \infty$, $\omega_2 = 0$ and $h_2 = 2$ (left) and $h_2 = 5$ (right)

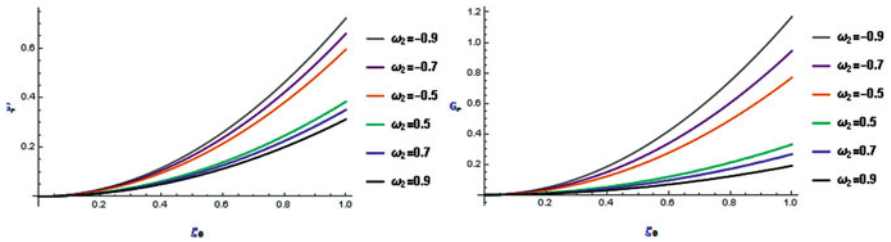

Fig. 2 G_r vs. ζ_0 plot for $r = 0.00129$, $h_1 \to \infty$, $\omega_1 = 0$ and $h_2 = 2$ (left) and $h_2 = 5$ (right)

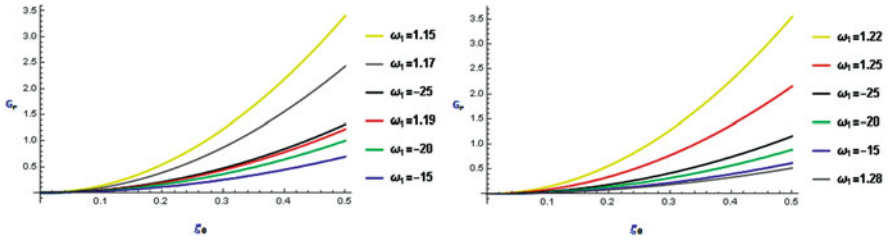

Fig. 3 G_r vs. ζ_0 plot for $r = 0.00129$, $h_2 \to \infty$, $\omega_2 = 0$ and $h_1 = 2$ (left) and $h_1 = 5$ (right)

finite values of h_1, h_2, ω_1, ω_2, and we observe that the breather span increases in space when h_1, h_2, ω_1, ω_2 increases for air–water interface and that the breather amplitude increases in time when h_1, h_2, ω_1, ω_2 decreases for the Boussinesq approximation.

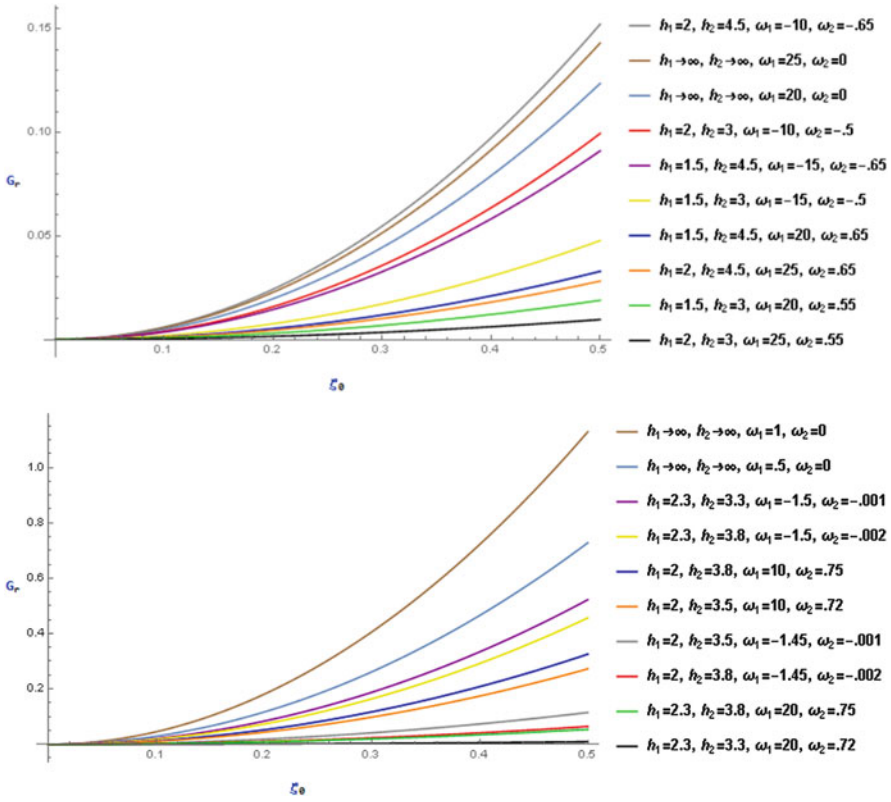

Fig. 4 G_r vs. ζ_0 plot for $r = 0.00129$ (left) and $r \to 1$ (right)

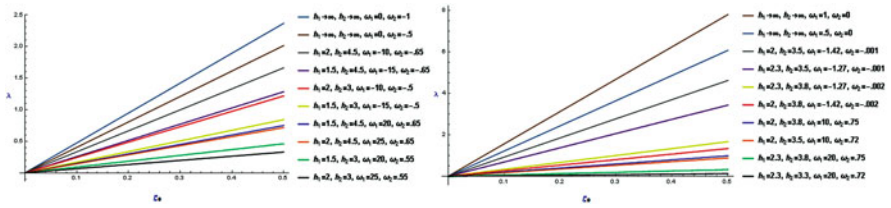

Fig. 5 λ vs. ζ_0 plot for $r = 0.00129$ (left) and $r \to 1$ (right). The region above each line indicates stable region and that of the below region indicates unstable region

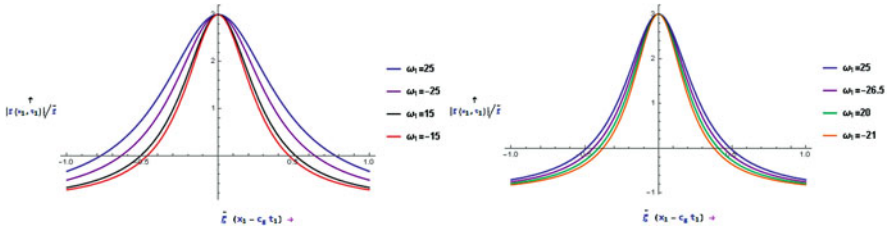

Fig. 6 $|\zeta(x_1, t_1)|/\tilde{\zeta}$ vs. $\tilde{\zeta}(x_1 - c_g t_1)$ plot for $r = 0.00129$, $h_1 \to \infty$, $\omega_2 = 0$ and $h_2 = 2$ (left) and $h_2 = 5$ (right)

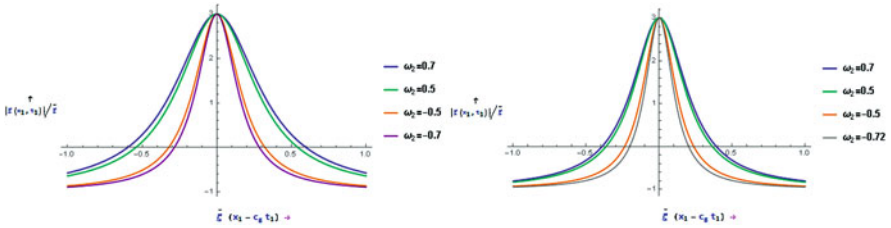

Fig. 7 $|\zeta(x_1, t_1)|/\tilde{\zeta}$ vs. $\tilde{\zeta}(x_1 - c_g t_1)$ plot for $r = 0.00129$, $h_1 \to \infty$, $\omega_1 = 0$ and $h_2 = 2$ (left) and $h_2 = 5$ (right)

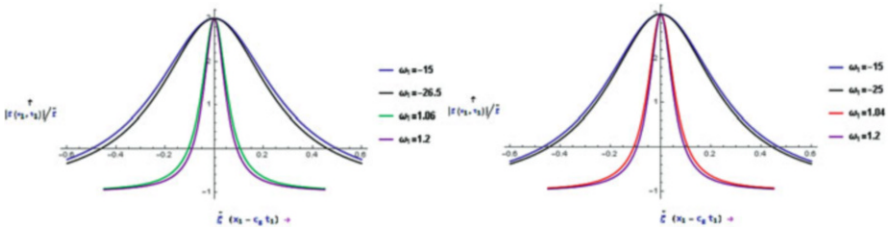

Fig. 8 $|\zeta(x_1, t_1)|/\tilde{\zeta}$ vs. $\tilde{\zeta}(x_1 - c_g t_1)$ plot for $r \to 1$, $h_2 \to \infty$, $\omega_2 = 0$ and $h_1 = 1.4$ (left) and $h_1 = 1.5$ (right)

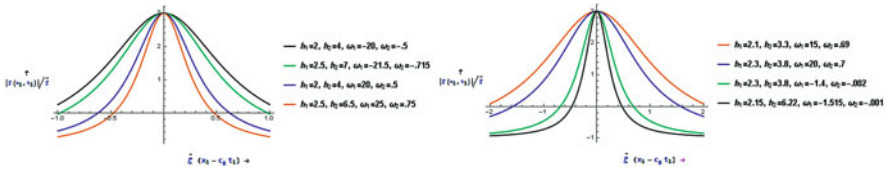

Fig. 9 $|\zeta(x_1, t_1)|/\tilde{\zeta}$ vs. $\tilde{\zeta}(x_1 - c_g t_1)$ plot for $r = 0.00129$ (left) and $r \to 1$ (right)

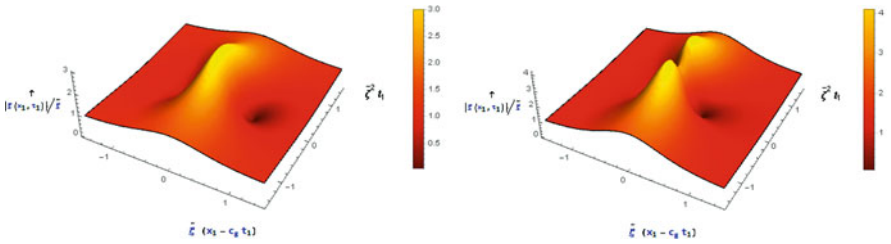

Fig. 10 The Peregrine Breather for $r = 0.00129$, $h_1 \to \infty$, $\omega_2 = 0$ and $h_2 = 2$, $\omega_1 = 20$ (left) and $h_2 = 5$, $\omega_1 = 20$ (right)

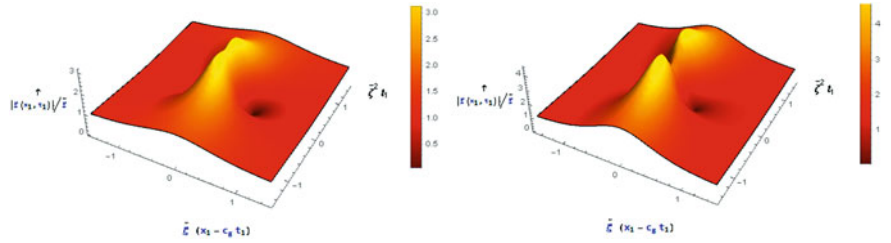

Fig. 11 The Peregrine Breather for $r = 0.00129$, $h_1 \to \infty$, $\omega_1 = 0$ and $h_2 = 3$, $\omega_2 = 0.65$ (left) and $h_2 = 5$, $\omega_2 = 0.65$ (right)

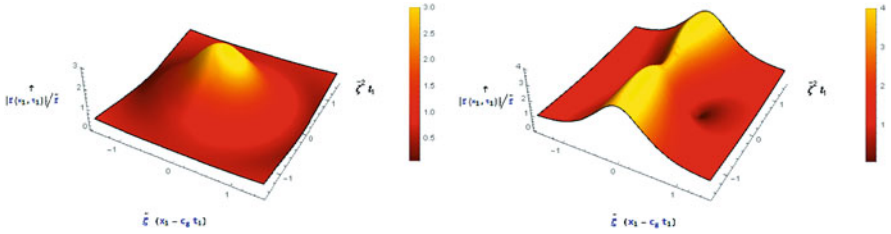

Fig. 12 The Peregrine Breather for $r = 0.00129$, $h_1 = 2$, $h_2 = 4$, $\omega_1 = 20$, $\omega_2 = 0.5$ (right) and $r \to 1$, $h_1 = 2.3$, $h_2 = 3.8$, $\omega_1 = 20$, $\omega_2 = 0.7$ (left)

Appendix

The coefficients appearing in Eq. (21) are

$$\begin{aligned}\alpha = \frac{1}{2}\left(\frac{dc_g}{dk}\right)_{k=1} &= \frac{1}{f_\sigma}[(\sigma_1 + r\sigma_2)c_g^2 \\ &+ \{2\sigma h_1(1-\sigma_1^2) + 2\sigma r h_2(1-\sigma_2^2) - (\omega_2 - r\omega_1)\delta_1\}c_g \\ &- \sigma^2\{\sigma_1 h_1^2(1-\sigma_1^2) + r\sigma_2 h_2^2(1-\sigma_2^2)\} \\ &- \{(\omega_2 - r\omega_1)\sigma + (1-r)\}(\delta_3 - \delta_4) - (1-r)\delta_1],\end{aligned}$$

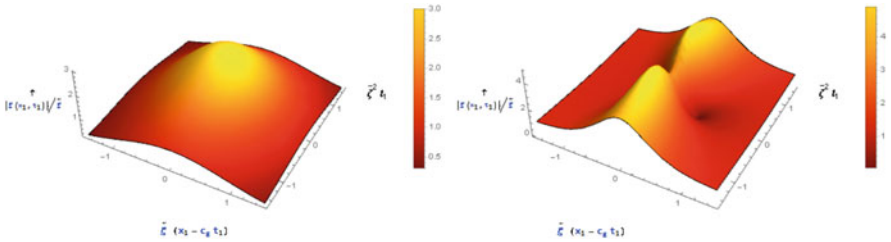

Fig. 13 The Peregrine Breather for $r = 0.00129$, $h_1 = 2.5$, $h_2 = 6.5$, $\omega_1 = 25$, $\omega_2 = 0.75$ (right) and $r \to 1$, $h_1 = 2.1$, $h_2 = 3.3$, $\omega_1 = 15$, $\omega_2 = 0.69$ (left)

$$\mu = \frac{1}{2\sigma_1^3\sigma_2^3 f_\sigma}\Bigg[\frac{2\{\sigma^2\sigma_1^2(1-\sigma_2^2) - r\sigma^2\sigma_2^2(1-\sigma_1^2) + \frac{\sigma_2\sigma_1^2\delta_5(c_g - h_2\omega_2)}{h_2} - \frac{r\sigma_1\sigma_2^2\delta_6(c_g + h_1\omega_1)}{h_1}\}^2}{\frac{c_g^2}{h_2} + \frac{rc_g^2}{h_1} - \delta_7}$$

$$+ \frac{\{\sigma^2\sigma_1^2(3-\sigma_2^2) - r\sigma^2\sigma_2^2(3-\sigma_1^2) - \omega_2\sigma_1^2\sigma_2(\delta_5 + \sigma + \sigma\sigma_2^2) - r\omega_1(\delta_6 + \sigma + \sigma\sigma_1^2)\}^2}{\sigma^2\sigma_2 + r\sigma^2\sigma_1}$$

$$- \frac{2\sigma_1^2\sigma_2^2(h_1\delta_5^2\sigma_1^2 + rh_2\delta_6^2\sigma_2^2)}{h_1h_2} - \sigma_1\sigma_2\{4\sigma^2\sigma_1^3(1-2\sigma_2^2) + 4r\sigma^2\sigma_2^3(1-2\sigma_1^2)$$

$$- \omega_2\sigma_2\sigma_1^3(4\sigma(1-\sigma_2^2) - \omega_2\sigma_2(1+\sigma_2^2))$$

$$+ r\omega_1\sigma_1\sigma_2^3(4\sigma(1-\sigma_1^2) + \omega_1\sigma_1(1+\sigma_1^2))\}],$$

$$\delta_1 = \sigma_1 h_2(1-\sigma_2^2) + \sigma_2 h_1(1-\sigma_1^2), \quad \delta_2 = \sigma_1 + h_1(1-\sigma_1^2),$$
$$\delta_3 = h_1h_2(1-\sigma_1^2)(1-\sigma_1^2),$$

$$\delta_4 = \sigma_1\sigma_2\{h_1^2(1-\sigma_1^2) + h_2^2(1-\sigma_2^2)\}, \delta_5 = 2\sigma - \sigma_2\omega_2, \delta_6 = 2\sigma + \sigma_1\omega_1,$$
$$\delta_7 = 1 - r + (\omega_2 - r\omega_1)c_g.$$

References

1. J.W. McLean, Y.C. Ma, D.U. Martin, P.G. Saffman, H.C. Yuen, Three-dimensional instability of finite-amplitude water waves. Phys. Rev. Lett. **46**, 817 (1981). https://doi.org/10.1103/PhysRevLett.46.817
2. H.C. Yuen, Nonlinear dynamics of interfacial waves. Phys. D Nonlinear Phenomena **12**(1–3), 71–82 (1984). https://doi.org/10.1016/0167-2789(84)90515-3
3. R. Grimshaw, D. Pullin, Stability of finite-amplitude interfacial waves. Part 1. Modulational instability for small-amplitude waves. J. Fluid Mech. **160**, 297–315 (1985). https://doi.org/10.1017/S0022112085003494

4. D. Pullin, R. Grimshaw, Stability of finite-amplitude interfacial waves. Part 3. The effect of basic current shear for one-dimensional instabilities. J. Fluid Mech. **172**, 277–306 (1986). https://doi.org/10.1017/S002211208600174X
5. A.K. Dhar, K.P. Das, Stability analysis from fourth order evolution equation for small but finite amplitude interfacial waves in the presence of a basic current shear. J. Austral. Math. Soc. Ser B. Appl. Math. **35**(3), 348–365 (1994). https://doi.org/10.1017/S0334270000009346
6. W. Choi, Nonlinear surface waves interacting with a linear shear current. Math. Comput. Simul. **80**(1), 29–36 (2009). https://doi.org/10.1016/j.matcom.2009.06.021
7. O.G. Nwogu, Interaction of finite-amplitude waves with vertically sheared current fields. J. Fluid Mech. **627**, 179–213 (2009). https://doi.org/10.1017/S0022112009005850
8. D.H. Peregrine, Water waves nonlinear Schrödinger equations and their solutions. Austral. Math. Soc. Ser. B. **25**, 16 (1983). https://doi.org/10.1017/S0334270000003891
9. B. Liao, G. Dong, Y. Ma, J.L. Gao, Linear-shear-current modified Schrödinger equation for gravity waves in finite water depth. Phys. Rev. E **96**, 043111 (2017). https://doi.org/10.1103/PhysRevE.96.043111